ADVANCED FUNCTIONAL MATERIALS
www.afm-journal.de

Oriented Growth and Assembly of Ag@C@Co Pentagonalprism Nanocables and their Highly Active Selected Catalysis Along the Edges for Dehydrogenation

Baolei Sun, Ming Wen, Qingsheng Wu,* and Jin Peng*

Magnetic double-shelled Ag@C@Co pentagonalprism nanocables are fabricated using a synchronous growth and oriented assembly process, in which the second shell of Co is arranged along the edges of Ag@C pentagonalprism nanowires (NWs). The resulting Ag@C@Co pentagonalprism nanocables exhibit an average diameter of ≈400 nm and consist of Ag core NWs with diameter of ≈200 nm and C middle layers with a thickness of ≈10 nm as well as outer Co shells with a thickness of ≈100 nm. UV-vis absorption spectroscopy shows that the Co shell on Ag@C NWs can damp the surface plasmon resonance (SPR) of the Ag core wires and lead to a red-shifted SPR absorption peak. Additionally, the Ag@C@Co nanocables have the ferromagnetic behavior, which can be controlled by modulating the shell density. The resulting magnetic Ag@C@Co nanocables exert excellent selected catalytic activity along the edges toward the dehydrogenation of ammonia borane aqueous under ambient conditions at room temperature.

1. Introduction

Much research work has been devoted to the fabrication of metallic composite nanoparticles (NPs) with core-shell architectures, in particular one dimensional (1D) bimetallic core-shell nanocables in recent years.[1–10] Induced by the intimate contact and the interaction between different components, together with the 1D core-shell structured architecture, the synergistic actions can generate the special properties,[11–21] such as unique magnetic, optical, electric, and catalytic properties, which are not available in their unary-core counterparts or alloy NPs. Additionally, containing a magnetic element in NPs is attractive owing to their applications on biomedical, information storage, technological, and catalytic applications.[22–30] Therefore, investigations on the synthesis and application of 1D magnetic core-shell nanocables are of great interest for harvesting the combined advantages of synergistic structural and electronic effects of 1D core-shell structure and the intrinsic property of the magnetic element. Besides the ferromagnetic behavior, Co included metallic heterogeneous structures can give the high catalysis activity for the hydrogen production, it may enable more diversified options for the recycling of nanocatalysts.

On the other hand, there are two aspects in the development of hydrogen powered society as a long-term solution for a secure energy future. Finding effective hydrogen storage materials is one of the difficult challenges.[31–33] Developing efficient recyclable catalysts for hydrogen release is another most important task need to overcome. Ammonia borane (NH_3BH_3, AB) has a hydrogen capacity of 19.6 wt%, exceeding that of gasoline, and becomes an attractive candidate for chemical hydrogen-storage applications.[34–37] How to practically apply this system is focused on the development of efficient recyclable catalysts to release hydrogen for further improving the kinetic and thermodynamic properties under moderate conditions.[38–45]

However, to the best of our knowledge, it has rarely been mentioned that exploring the synthesis and application of 1D magnetic bimetallic pentagonalprism shaped nanocables with carbon separated double-shelled structure,[46–49] which further clarify the oriented distribution affects on the novel properties along edges. Therefore, it is of great importance for the development of the fabrication strategy, properties, and applications of bimetallic magnetic nanocables along surface edges.

In this work, the new designed bimetallic magnetic Ag@C@Co pentagonalprism nanocables are constructed through synchronous growth and directional assembly process in reflux reaction system, in which the tunable outer shell of Co NPs are arranged along the edges of Ag@C pentagonalprism nanowires (NWs). The effects of the double-shell structure and directional shell density on their optic, magnetic and catalytic properties have been investigated in present work. It can be seen that Ag@C@Co nanocables not only provide a magnetic property but also furnish excellent catalytic ability toward the dehydrogenation of AB aqueous under ambient atmosphere at room temperature.

2. Results and Discussion

2.1. Proposed Mechanism of Formation

Based on synchronous grown Ag@C NWs with the amorphous C shell thickness of ≈10 nm (Supporting Information,

B. Sun, Prof. M. Wen, Prof. Q. S. Wu, J. Peng
Department of Chemistry
Tongji University
1239 Siping Road, Shanghai 200092, P.R. China
E-mail: m_wen@tongji.edu.cn; qswu@tongji.edu.cn

DOI: 10.1002/adfm.201200274

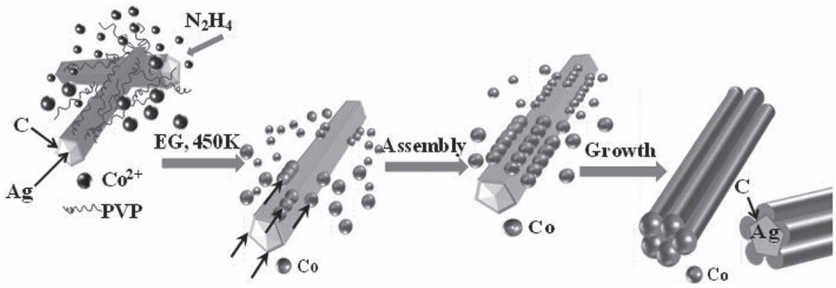

Figure 1. Schematic illustration of Ag@C@Co pentagonalprism nanocables fabricated through the directional growth and assembly process.

Figure S1), Ag@C@Co pentagonalprism nanocables are synthesized through oriented assembly process, in which Co NPs are oriented along the edges, and shown in **Figure 1**. In the presence of NaOH (≈1.2 mmol), the directional assembly of Ag@C@Co pentagonalprism nanocables is performed through the reduction of $CoCl_2 \cdot 6H_2O$ by hydrazine hydrate in ethylene glycol solution involving PVP as surfactant in the reflux reaction system at ≈450K for 30 min. The oriented growth and assembly process has been examined and monitored by UV-vis spectra withdrawing samples at different reaction stages, which is proposed as illustrated in Figure 1. By reacting Co^{2+} in hydrazine solution, a dark blue complex of $[Co(N_2H_4)_3]^{2+}$ is formed.[50–52] Under reflux treatment at the boiling point of the ethylene glycol (≈450K), the excess hydrazine reduces the $[Co(N_2H_4)_3]^{2+}$ complex into small Co NPs.[53,54] In the presence of NaOH, the assembly of Co NPs was directed along the five edges of Ag@C pentagonalprism NWs, resulting from either their high surface energy or the magnetic effects, and finally give rise to Ag@C@Co nanocables with the surface shell shape of five Co edges. The scanning electron microscope (SEM) images obtained at different reaction stage agree with the proposed formation process (Supporting Information, Figure S2). The assumption has also immediately been confirmed by monitoring the UV-vis spectra (Supporting Information, Figure S3). A distinct peak, which arises from the surface plasmon absorption by Ag, can be observed in trace (a) for Ag@C NWs. Because of the broad and strong absorption of Co shell in the same spectral region as Ag cores, the intensity of this characteristic peak decrease quickly in trace (b) and almost disappears completely in trace (c) for Co NPs partial and full covered Ag@C@Co nanocables, respectively.

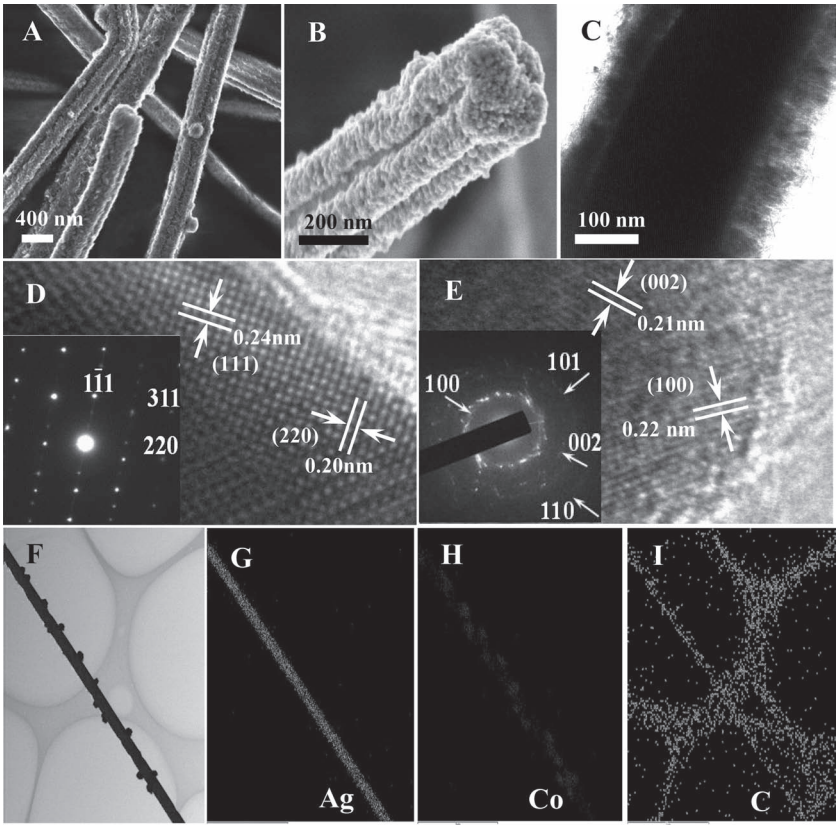

Figure 2. A) SEM image of Ag@C@Co nanocables; B) magnification SEM, and C) TEM images of a single Ag@C@Co nanocable. D) HRTEM image of Ag nanowire with inset SADP; E) HRTEM image of Co shell with inset SADP; F) BF-STEM image of a single partial Co nanoparticles covered Ag@C@Co nanocable; and G–I) elemental maps for Ag, Co, and C of a single sparse Co nanoparticles covered Ag@C@Co nanocable. The TEM Cu grid is covered by C.

2.2. Morphologies and Structures

The SEM and transmission electron microscopy (TEM) images of the Ag@C@Co nanocables are shown in **Figure 2**. The products are pentagonalprism nanocables in shape with an average diameter of ≈400 nm (Figure 2A). In magnification SEM images in Figure 2B, it can be observed that Co NPs arrange along the five edges of Ag@C pentagonalprism nanowires. A distinct contrast of core and shell layer metals can be observed clearly in TEM image in Figure 2C, the dark cores nanowire is Ag (≈200 nm) and the gray shell layers are including C (≈10 nm) and Co (≈100 nm). The high-resolution TEM (HRTEM) image (Figure 2D) of Ag core NW present the crystalline structure with lattice spacing of 0.24 nm and 0.20 nm corresponding to Ag (111) and (220) planes spacing, respectively. In the inset of Figure 2D, the selected-area electron diffraction pattern (SADP) recorded from single Ag core NW exhibits the single crystal diffraction pattern with the indexed plane of (1–11), (311) and (220). The HRTEM image in Figure 2E shows the continuous Co shells with the lattice spacing of 0.21 nm and 0.22 nm are corresponding to the identity distance of (002) and (100) planes in Co hexagonal close packed (hcp) structure. The SADP for the Co shell presents clear crystalline spot ring (Figure 2E inset), which corresponds to the polycrystalline structure with

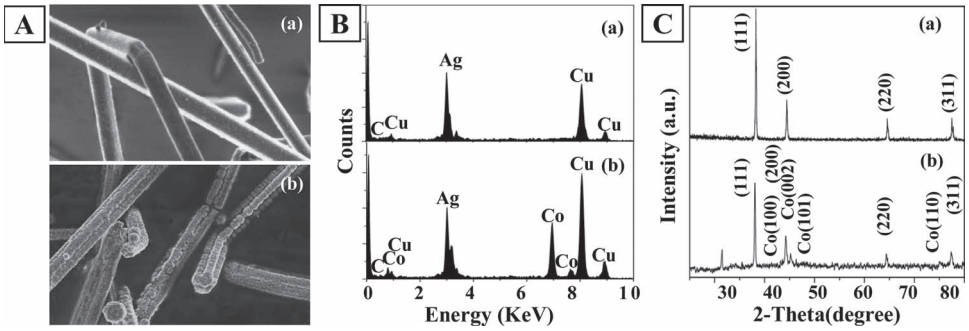

Figure 3. SEM images (A), EDS (B), and XRD patterns (C) of Ag@C nanowires (a) and Ag@C@Co nanocables (b). Cu is from the TEM grid.

the indexed plane of (100), (101), (002) and (110), indicating that Co is isolated as NPs and assembly arround the surface of Ag@C nanowires. In order to clearly understand the elemental distribution of the as-designed nanocables, a single sparse Co arranged Ag@C@Co nanocable obtained in the earlier reaction stage is characterized by bright field scanning TEM (BF-STEM). Figure 1F shows a representative STEM image. Figure 1G–I illustrate the corresponding energy dispersive X-ray spectroscopy (EDS) maps for Ag, Co, and C, confirming that C layer covered on the Ag NWs and the Co NPs deposited on the surface. Thus the products are layer-by-layer double-shelled Ag@C@Co nanocables.

Figure 3 exhibits the morphologies of Ag@C NWs (Figure 3A(a)) and Ag@C@Co (Figure 3A(b)) nanocables together with their corresponding EDS analysis and the X-ray diffraction (XRD) patterns. In Figure 3B, the EDS analysis of Ag@C (trace (a)) nanowires only shows Ag with a small amount of C and that of Ag@C@Co (trace (b)) nanocables reveals that the Ag/Co atomic ratio to be ≈1:1, which agree well with the target atomic ratio. Furthermore, the EDS analysis of Ag@C@Co obtained in different reaction stages were examined and given in Figure S4 (Supporting Information). It illustrated that the as-obtained products consist of Ag and Co within the different atom ratio, which Co content increases with the increase of reaction time. The XRD pattern of as-prepared Ag@C@Co nanocables shown in Figure 3C agrees well with the fcc (face centered cubic) lattice of Ag NWs core (JCPDF#04-0783) and hcp (hexagonal close packed) lattice Co NPs shells (JCPDF#01-1277), confirming the fabrication of layer-by-layer heterostructured Ag@C@Co double-shell nanocables.

To further confirm the 1D double-shell architecture, X-ray photoelectron spectroscopy (XPS) was also applied to the prepared nanocables. The XPS spectra for the surface of Ag@C nanowires and Ag@C@Co nanocables obtained in different reaction periods are presented in **Figure 4**, in which the numbers of emitted photoelectrons are given as a function of binding energy up to 1100 eV. The emission from the inelastic collisions of photoelectrons gives rise to a general background. It can be observed that the Ag@C nanowires present three photoemission peaks (Ag3d, C1s and O1s) in Figure 4A. Then,

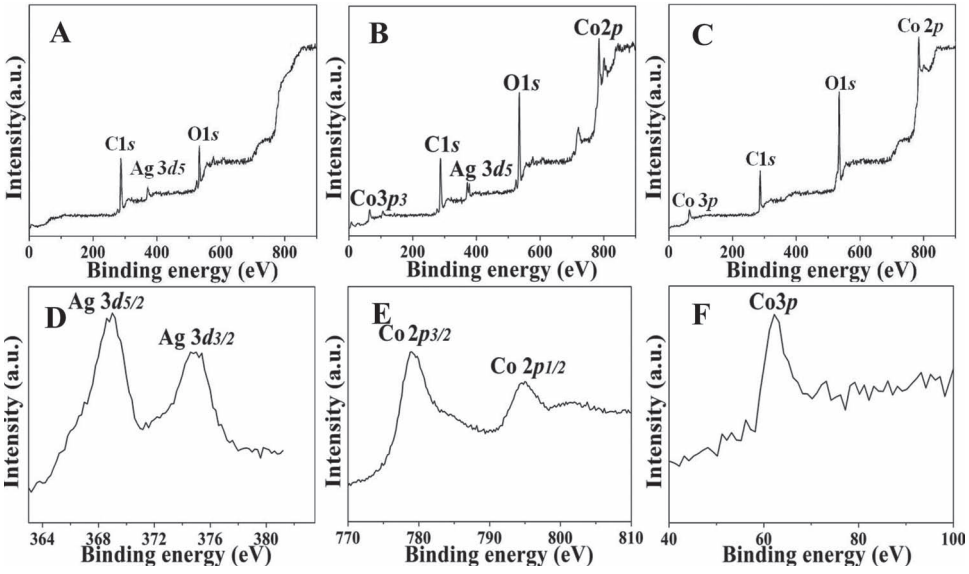

Figure 4. XPS spectra of Ag@C nanowires (A), Co partial covered Ag@C@Co nanocables (B), and Co full covered Ag@C@Co nanocables (C), with detailed spectra of Ag 3d (D), Co 2p (E) and Co 3p (F).

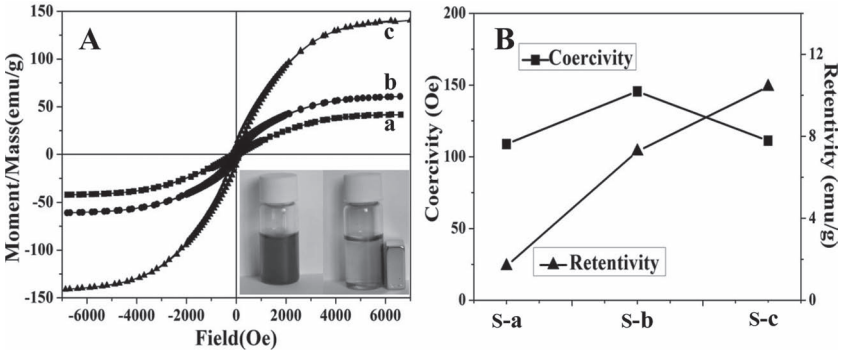

Figure 5. Magnetic behaviors: A) Room-temperature hysteresis loops of Ag@C@Co nanocables with partial covered Co (a) and full covered Co (b) as well as Co nanoparticles (c). Inset: Photographs of the Ag@C@Co nanocables suspended in the aqueous solution quickly response to a magnet. B) The variations of *Hc* and *Mr* with different Co content for Ag@C@Co nanocables with partial covered Co (S-a) and full covered Co (S-b) as well as Co nanoparticles (S-c)

as the assembly of Co partial covered on Ag@C pentagonal-prism nanowires, five peaks of Ag3d, Co 2p, Co 3p, C1s and O1s appear in Figure 4B. Eventually, the Ag3d peak disappeared in Figure 4C due to the full covering of Co in the final Ag@C@Co nanocables. Magnified Ag 3d peaks in Figure 4D, which consist of two sharp peaks at 368.71 and 374.84 eV, are due to the spin-orbit splitting of $3d_{5/2}$ and $3d_{3/2}$, respectively. The spin-orbit doublet splitting value of the 3d core level, corresponding to the differences of binding energies (BE) between $3d_{5/2}$ and $3d_{3/2}$, was estimated to be 6.13 eV, indicating that Ag(0) is dominant. Magnified Co 2p peaks in Figure 4E, two peaks resulted by the 2p electrons multiplet-splitting are $2p_{3/2}$ and $2p_{1/2}$ with BE values of 782.08 and 797.29 eV, implying for Co(II) and Co(0). Co 3p has BE values of 61.95 eV, implying for Co(0) (Figure 4F). In addition, the O 1s peak of 531.87 eV implied that oxygen (O^{2-}) species existed on the surface of the nanoparticles, confirmed the oxides of silver and cobalt. In the *Binding Energy Lookup Table for Signals from Elements and Common Chemical Species*, C1s = 285.0 eV, $Co2p_{3/2}$ = 780.0 eV, $Co2p_{1/2}$ = 795.5 eV, Co3p = 59.0 eV, $Ag3d_{5/2}$ = 367.9 eV, and $Ag3d_{3/2}$ = 373.9 eV.[55] The signals of metallic bonding energy in as-obtained Ag@C@Co nanocables are slightly shift. The reason is suggested to be that the environment of cobalt and silver in Ag@C@Co nanocables is different from pure silver and cobalt metals, and results in the signals shift of metallic bonding energy.

In addition, NaOH and polyvinylpyrrolidoneK-30 (PVP) play a crucial role in the formation of Ag@C@Co pentagonalprism nanocables. If NaOH is absent, no Co NPs or only a small amount of Co NPs are deposited on the surface of Ag@C NWs at random (Supporting Information, Figure S5). When the molar ratio of PVP:M^{2+} changes from 0.05 to 0.25, the shape of Co on the surface changes from plate to particles due to the space limitation from PVP (Supporting Information, Figure S6). The oriented density of Co NPs could be controlled by varying the molar ratio between Ag@C and Co (Supporting Information, Figure S7) at above optimized concentration of NaOH and PVP. Moreover, a reaction time over 90 min will lead to the shape of Co shells change from flowerlike nanoplates to NPs (Supporting Information, Figure S8).

2.3. Magnetic Property

Measurements of magnetization versus applied field for Ag@C@Co nanocables and Co NPs are ploted in **Figure 5** and the detail data are summarized in Table S1 (Supporting Information). Ag@C NWs cannot give rise to the magnetic hysteresis loops. In contrast, the morphology of Co NPs with its XRD and EDS is characterized and illustrated in Figure S9 (Supporting Information). In Figure 5A, the saturation magnetization (*Ms*) of Ag@C@Co with full and half covered Co shell are 60.81 and 41.94 emu g^{-1}, respectively. Although these values are lower than that (140.84 emu g^{-1}) of the Co NPs, it does not affect the magnetic recyclability of the double-shelled nanocables. In our case, the as-prepared Ag@C@Co nanocables, suspended in the aqueous solution, can quickly respond to a magnet (Figure 5A inset) and thus can be easily separated and recovered by an external magnet. The variations of coercivity (*Hc*) and retentivity (*Mr*) for partial or full Co covered Ag@C@Co nanocables and Co NPs are illustrated in Figure 5B. The content of Co is proportional to the *Mr* due to its atomic magnetic dipole moment, and the full Co covered Ag@C@Co nanocables have the largest *Hc* of 145.60 Oe. Thus, the magnetic behavior can be changed with the variation of distribution density of Co.

2.4. Catalytic Properties

Since ammonia borane (AB) is a promising chemical hydrogen storage material, the catalytic properties of the as-obtained Ag@C@Co nanocables have been investigated for hydrolytic dehydrogenation toward AB. The hydrolysis of NH_3BH_3 can be briefly expressed as follows:

$$NH_3BH_3(aq) + 2H_2O \xrightarrow{\text{Catalysts}} NH_4^+(aq) + BO_2^-(aq) + 3H_2(g) \quad (1)$$

Figure 6 shows the amount of H_2 generated as a function of reaction time by employing different as-synthesized catalysts. Compared with Ag@C NWs and Co NPs, the Ag@C@Co pentagonalprism nanocables exhibit markedly high selected catalytic activity along the edges to complete dehydrogenation reaction of AB within 25 min, as shown in curve (a) in Figure 6A. The H_2 bubbles generated from edges can be clearly observed from photograph inset of **Figure 7**. This excellent catalytic activity is much higher than that of the pure Co NPs (curve (b), 100 min). Because of the protection of C shell, Ag@C NWs cannot be found any catalytic activity (curve (c)) although noble metal Ag should present the catalysis activity in normal case. Due to surface confinement during the growth process, the size of Co NPs on the surface of Ag@C@Co pentagonalprism nanocables is smaller than that of as-contrast sample of Co NPs (Figure S9, Supporting Information). An advantage of this nanocable architecture is that Co NPs catalytic centers are oriented along the long axial direction, and the width of the surface d-band of Co NPs edges can be modified by the interaction between the three kinds of atoms in relation to the strain

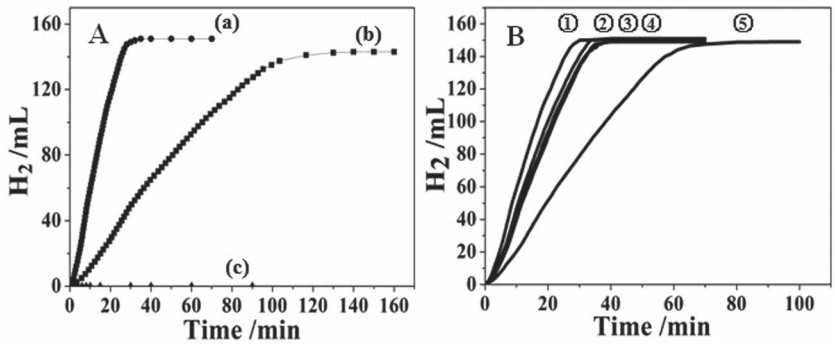

Figure 6. A) Hydrogen generation from AB aqueous (0.13 M, 20 mL) catalyzed by Ag@C@Co nanocables (a), Co NPs (b), and Ag@C NWs (c) under under ambient atmosphere at room temperature. B) Hydrogen generation from above AB aqueous solution catalyzed by Ag@C@Co nanocables from the first to fifth run of the lifetime experiment under ambient atomosphere at toom temperature. Catalyst/AB = 0.023 (molar ratio).

and ligand effects,[7,56–58] thus the high activity edges consisted of small sized Co NPs lead to high actively selected catalysis along edges of Ag@C@Co pentagonalprism nanocables for dehydrogenation toward AB, and this is illustrated in the shematic view in Figure 7. Additionally, the lifetime and stability of the as-synthesized Ag@C@Co nanocables were investigated in the present work. We tested the catalytic activity of the Ag@C@Co nanocables five times for hydrolytic dehydrogenation toward AB solution under ambient atmosphere at room temperature. As shown in Figure 6B, the small decrease of the catalytic activity for the Ag@C@Co pentagonalprism nanocables can be observed over five experiments. From the first to the fourth, the reaction time only increased a small amount from 25 min to 30 min, and the fifth reaction process spends about 60 min. Therefore, the as-obtained Ag@C@Co nanocables have the relative good lifetime and stability for the hydrolytic hydrogen generation of AB under ambient atmosphere. In addition, the as-obtained pentagonalprism Ag@C@Co nanocables also give rise to excellent catalytic activity for the hydrogen generation in KBH_4 (Supporting Information, Figure S10).

3. Conclusion

In conclusion, novel magnetic double-shelled Ag@C@Co pentagonalprism nanocables have been successfully fabricated through an oriented growth and assembly process. The assembly of Co NPs prefers to orient along the edges of Ag@C pentagonal-prism NWs cores. In addition to possessing easy recovery functions due to its magnetic properties, the resultant Ag@C@Co nanocables exhibit highly efficient selected catalytic activity along the edges for the hydrolytic dehydrogenation toward AB under ambient atmosphere at room temperature. Moreover, this rational and general method can be easily extended to the other metallic systems, which are used as optical, magnetic, and electrical materials as well as heterogeneous catalysts.

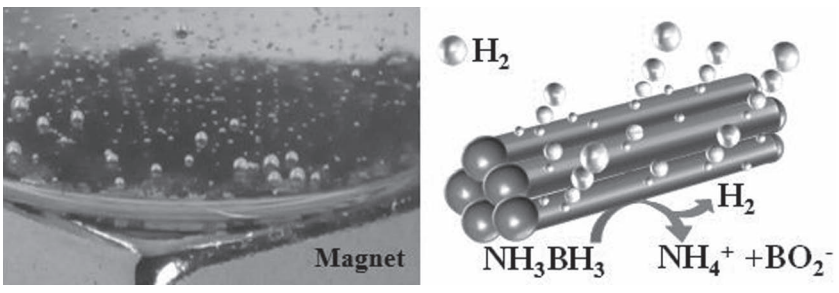

Figure 7. The photograph (left) and schematic view (right) of high active selected catalysis along edges of Ag@C@Co pentagonalprism nanocables for dehydrogenation toward ammonia borane.

4. Experimental Section

Chemicals: Ammonia borane (AB, NH_3BH_3, 90%) was purchased from Aldrich, potassium borohydride (KBH_4, 95%), sodium chloride (NaCl, 99.5%), silver nitrate ($AgNO_3$, 99.8%), glucose ($C_6H_{12}O_6 \cdot H_2O$), ammonia solution (25 ≈28%), sodium hydroxide (NaOH, 99%), polyvinylpyrrolidone K-30 (PVP, $(C_6H_9NO)_n$, Mw: av. 40000), cobalt (II) chloride hexahydrate ($CoCl_2 \bullet 6H_2O$, 99%), ethylene glycol (EG, 99%), hydrazine hydrate (N_2H_4, 85%), and ethanol (C_2H_5OH, 99.7%), were purchased from Sinopharm Chemical Reagent Co., Ltd. (SCRC). All the reagents used in this work were used as received without further purification.

Synchronous Growth of Ag@C Nanowires: The Ag@C core-shell nanowires were prepared according to previous reports.[59] In a typical experiment, 2.5 mL silver nitrate (0.02 M) and 2.5 mL sodium chloride (0.02 M) were added to 10 mL distilled water to form silver chloride colloidal solution. 0.006 g glucose was dissolved into the above colloidal solution and the mixture was transferred into and sealed in stainless steel autoclave with a Teflon liner of 20 mL capacity. The autoclave was then slowly heated up to 453 K with a rate of 2 K min^{-1} and maintained 18 h. After the autoclave was air cooled down to room temperature naturally, the resulting silver-gray precipitate was filtered and washed with deionized water, dilute ammonia solution (0.1 M), and absolute ethanol, and then dried under vacuum at 333 K for 2 h for further synthesis of Ag@C@Co nanocables.

Synthesis of Ag@C@Co Nanocables: Typically, 48.70 mg NaOH, 25.5 mg PVP, 1.0 mg Ag NWs (dispersed in 0.4 mL ethanol), and 0.27 mL of an EG solution of $CoCl_2 \cdot 6H_2O$ (0.042 M) were added into a four-necked round-bottom flask with 10 mL EG and kept for 2 h under electric stirring at room temperature. Then the mixture was slowly heated. When the temperature rose to 323 K, 83 μL hydrazine hydrate was dropwise injected into the refluxing mixture. The mixture was sequentially heated up to 450 K and kept for 30 min. After cooling to room temperature, the resulting black precipitate was washed with ethanol and deionized water to remove residual EG and PVP. The washed black precipitate was dispersed in ethanol for further characterization. The synthesis progress was traced by UV-vis spectra. Their corresponding compositions were measured by EDS and shown in Supporting Information Figure S4.

Synthesis of Co Nanoparticles: In a typically method, 51 mg PVP, 0.5 mL of an EG solution of $CoCl_2 \cdot 6H_2O$ (0.042 M) were added into a four-necked round-bottom flask with 10 mL EG and kept 30 min under electric stirring at room temperature. Then the mixture was slowly heated. When the temperature rose to 323 K, 83

μL hydrazine hydrate was dropwise injected into the refluxing mixture. The mixture was sequentially heated up to 450 K and kept for 15 min. After cooling to room temperature, the resulting black precipitate was washed with ethanol and deionized water to remove residual EG and PVP. The washed black precipitate was dispersed in ethanol for further characterization.

Characterization: Field-emission scanning electron microscopy (FE-SEM, JEOL, S-4800) was applied to investigate the size and morphology of the samples. For the detailed microstructure study, Transmission electron microscopy (TEM) and high-resolution TEM (HRTEM) images were taken on a JEOL JEM-1200EX microscope.

Scanning transmission electron microscopy (STEM) and elemental mapping were carried out under the bright field (BF) mode on a JEOL JEM-2100 F microscope. The composition information was conducted by energy dispersive X-ray spectroscopy (EDS) at 20 keV on a TN5400 EDS instrument (oxiford).

Powder X-ray diffraction (XRD) was performed on a Bruker Foucs D8 (Germany) diffractometer with a Cu Kα X-ray radiation source (λ = 0.154056 nm). A glass substrate holding the powder sample was covered by an adhesive tape on the surface to prevent the sample from exposure to air during the measurements.

X-ray photoelectron spectroscopy (XPS) experiments were carried out on a RBD upgraded PHI-5000C ESCA system (Perkin Elmer) using a Al Kα radiation ($h\nu$ = 1486.6 eV). In general, the X-ray anode was run at 250 W and the high voltage was kept at 14.0 kV with a detection angle of 54°. The pass energy was fixed at 23.5, 46.95, or 93.90 eV to ensure sufficient resolution and sensitivity. The base pressure of the analyzer chamber was about 5×10^{-8} Pa. The sample was directly pressed to a self-supported disk (10 mm × 10 mm) and mounted on a sample holder then transferred into the analyzer chamber. The entire spectra (from 0 to 1100 eV) and the narrow spectra of all the elements with much higher resolution were both recorded by using RBD 147 interface (RBD Enterprises, USA) through the AugerScan 3.21 software. Binding energies were calibrated by using the containment carbon (C1s = 284.6eV). The data analysis was carried out using the RBD AugerScan 3.21 software provided by RBD Enterprises or XPSPeak4.1 provided by Raymund W.M. Kwok (The Chinese University of Hongkong, China).

UV–vis spectra of the samples (dispersed into absolute ethanol) were recorded using a Agilent-8453 ultraviolet visible spectrophotometer.

Vibration sample magnetometer (VSM) was used to examine the magnetic properties of as-synthesized products on lakeshore-735 instrument.

Catalysis Test for Hydrogen Generation: To study the catalytic properties of the as-synthesized products, their catalytic activities were evaluated for the dehydrogenation of AB in aqueous solution. In a typical experiment, 20 mL of NH_3BH_3 solution (0.13 M), 5 mL deionized water were added to a three-necked round-bottom flask. One neck was connected to a gas burette through soft rubber tube. Then, catalysts (5.0 mg Ag@C@Co nanocomposites, 3.5 mg Co NPs, 6.4 mg Ag NWs, keeping the molar of each catalyst equal) were added into the reaction solution rapidly and kept every pipe orifice was sealed. The reaction was started and performed under constant electric stirring at room temperature. The volume of hydrogen gas generated from the hydrolysis reaction was measured using the water-displacement method.

Supporting Information

Supporting Information is available from the Wiley Online Library or from the author.

Acknowledgements

This work was financially supported by the National Natural Science Foundation of China (Nos: 21171130, 51072134 and 91122025), Innovation Program of SECF (10ZZ21), and 973 Project of China (No: 2011CB932404).

Received: January 30, 2012
Revised: February 25, 2012
Published online: April 24, 2012

[1] S. L. Tripp, S. V. Pusztay, A. Wei, *J. Am. Chem. Soc.* **2002**, *124*, 7914.
[2] D. S. Wang, Y. D. Li, *J. Am. Chem. Soc.* **2010**, *132*, 6280.
[3] Q. Yuan, Z. Y. Zhou, J. Zhuang, X. Wang, *Chem. Mater.* **2010**, *22*, 2395.
[4] D. T. Schoen, A. P. Schoen, L. Hu, H. S. Kim, S. C. Heilshorn, Y. Cui, *Nano Lett.* **2010**, *10*, 3628.
[5] M. J. Hu, Y. Lu, S. Zhang, S. H. Yu, *J. Am. Chem. Soc.* **2008**, *130*, 11606.
[6] Y. W. Lee, M. Kim, Z. H. Kim, S. W. Han, *J. Am. Chem. Soc.* **2009**, *131*, 17036.
[7] F. Tao, M. E. Grass, Y. W. Zhang, D. R. Butcher, J. R. Renzas, Z. Liu, J. Y. Chung, B. S. Mun, M. Salmeron, G. A. Somorjai, *Science* **2008**, *322*, 932.
[8] S. Alayoglu, A. U. Nilekar, M. Mavrikakis, B. Eichhorn, *Nat. Mater.* **2008**, *7*, 333.
[9] R. W. J. Scott, O. M. Wilson, S. K. Oh, E. A. Kenik, R. M. Crooks, *J. Am. Chem. Soc.* **2004**, *126*, 15583.
[10] M. P. Mallin, C. J. Murphy, *Nano Lett.* **2002**, *2*, 1235.
[11] Y. J. Xiong, J. M. McLellan, J. Y. Chen, Y. D. Yin, Z. Y. Li, Y. N. Xia, *J. Am. Chem. Soc.* **2005**, *127*, 17118.
[12] C. Gu, T. Y. Zhang, *Langmuir* **2008**, *24*, 12010.
[13] X. D. Wang, J. H. Song, J. Liu, Z. L. Wang, *Science* **2007**, *316*, 102.
[14] B. Wang, J. S. Chen, H. B. Wu, Z. Y. Wang, X. W. Lou, *J. Am. Chem. Soc.* **2011**, *133*, 17146.
[15] H. Q. Yan, R. R. He, J. Pham, P. D. Yang, *Adv. Mater.* **2003**, *15*, 402.
[16] T. Zhang, W. Dong, M. Keeter-Brewer, S. Konar, R. N. Njabon, Z. R. Tian, *J. Am. Chem. Soc.* **2006**, *128*, 10960.
[17] Y. H. Leung, A. B. Djurisic, J. Gao, M. H. Xie, W. K. Chan, *Chem. Phys. Lett.* **2004**, *385*, 155.
[18] H. Zeng, S. Sun, *Adv. Funct. Mater.* **2008**, *18*, 391.
[19] X. Zheng, S. Yuan, Z. Tian, S. Yin, J. He, L. Liu, *Chem. Mater.* **2009**, *21*, 4839.
[20] J. M. Yan, X. B. Zhang, M. Haruta, Q. Xu, *J. Am. Chem. Soc.* **2010**, *132*, 5326.
[21] S. K. Poznyak, D. V. Talapin, H. Weller, *Nano Lett.* **2004**, *4*, 693.
[22] J. Kim, C. Rong, Y. Lee, J. P. Liu, S. Sun, *Chem. Mater.* **2008**, *20*, 7242.
[23] H. Zhang, J. Ding, G. Chow, M. Ran, J. Yi, *Chem. Mater.* **2009**, *21*, 5222.
[24] A. H. Lu, E. L. Salabas, F. Schuth, *Angew. Chem. Int. Ed.* **2007**, *46*, 1222.
[25] N. C. King, R. A. Blackley, M. L. Wears, D. M. Newman, W. Z. Zhou, D. W. Bruce, *Chem. Commun.* **2006**, *32*, 3414.
[26] F. J. Himpsel, J. E. Ortega, G. J. Mankey, R. F. Willis, *Adv. Phys.* **1998**, *47*, 511.
[27] M. Wen, F. Zhang, M. Z. Cheng, Q. S. Wu, B. L. Sun, Y. Z. Sun, *Chem. Phys. Chem.* **2011**, *12*, 3573.
[28] F. Zhang, M. Wen, M. Z. Cheng, Q. S. Wu, X. G. Meng, *J. Mater. Chem.* **2010**, *20*, 7661.
[29] M. Wen, D. Yang, Q. S. Wu, R. P. Lu, Y. Z. Zhu, *Chem. Commun.* **2010**, *46*, 219.
[30] M. Wen, X. G. Meng, B. L. Sun, Q. S. Wu, X. L. Chai, *Inorg. Chem.* **2011**, *50*, 9393.
[31] W. Grochala, P. P. Edwards, *Chem. Rev.* **2004**, *104*, 1283.
[32] P. Chen, Z. Xiong, J. Luo, J. Lin, K. L. Tan, *Nature* **2002**, *420*, 302.
[33] L. Schlapbach, A. Zuttel, *Nature* **2001**, *414*, 353.

[34] A. Gutowska, L. Y. Li, Y. S. Shin, C. M. M. Wang, X. H. S. Li, J. C. Linehan, R. S. Smith, B. D. Kay, M. Gutowski, T. Autrey, *Angew. Chem. Int. Ed.* **2005**, *44*, 3578.
[35] D. W. Himmelberger, C. W. Yoon, M. E. Bluhm, P. J. Carroll, L. G. Sneddon, *J. Am. Chem. Soc.* **2009**, *131*, 14101.
[36] B. L. Davis, D. A. Dixon, E. B. Garner, J. C. Gordon, M. H. Matus, B. Scott, F. H. Stephens, *Angew. Chem. Int. Ed.* **2009**, *48*, 6812.
[37] F. H. Stephens, R. T. Baker, M. H. Matus, D. J. Grant, D. A. Dixon, *Angew. Chem. Int. Ed.* **2007**, *46*, 746.
[38] R. J. Keaton, J. M. Blacquiere, R. T. Baker, *J. Am. Chem. Soc.* **2007**, *129*, 1844.
[39] M. C. Denney, V. Pons, T. J. Hebden, D. M. Heinekey, K. I. Goldberg, *J. Am. Chem. Soc.* **2006**, *128*, 12048.
[40] M. E. Bluhm, M. G. Bradley, R. Butterick, U. Kusari, L. G. Sneddon, *J. Am. Chem. Soc.* **2006**, *128*, 7748.
[41] J. M. Yan, X. B. Zhang, S. Han, H. Shioyama, Q. Xu, *Angew. Chem. Int. Ed.* **2008**, *47*, 2287.
[42] T. J. Clark, G. R. Whittell, I. Manners, *Inorg. Chem.* **2007**, *46*, 7522.
[43] M. Chandra, Q. Xu, *J. Power Sources.* **2007**, *168*, 135.
[44] A. Paul, C. B. Musgrave, *Angew. Chem. Int. Ed.* **2007**, *46*, 8153.
[45] C. W. Yoon, L. G. Sneddon, *J. Am. Chem. Soc.* **2006**, *128*, 13992.
[46] Y. H. Xu, J. P. Wang, *Adv. Mater.* **2008**, *20*, 994.
[47] W. S. Choi, H. Y. Koo, D. Y. Kim, *Adv. Mater.* **2007**, *19*, 451.
[48] W. R. Lee, M. G. Kim, J. R. Choi, J. I. Park, S. J. Ko, S. J. Oh, J. Cheon, *J. Am. Chem. Soc.* **2005**, *127*, 16090.
[49] J. I. Park, J. Cheon, *J. Am. Chem. Soc.* **2001**, *123*, 5743.
[50] We. Z. Wang, S. L. Xiong, Z. D. Zhang, *Crystal Growth Design* **2006**, *6*, 2422.
[51] V. F. Puntes, K. M. Krishnan, A. P. Alivisatos, *Science* **2001**, *291*, 2115.
[52] D. H. Chen, C. H. Hsieh, *J. Mater. Chem.* **2002**, *12*, 2412.
[53] X. L. Hu, J. C. Yu, *Chem. Mater.* **2008**, *20*, 6743.
[54] N. Wang, X. Cao, D. S. Kong, W. M. Chen, L. Guo, C. P. Chen, *J. Phys. Chem. C* **2008**, *112*, 6613.
[55] B. V. Crist, *PDF Handbook of Elements and Native Oxides*, XPS International, LCC,Mountain ViewCA, **1999**.
[56] J. R. Kitchin, J. K. Norskov, M. A. Barteau, J. G. Chen, *Phys. Rev Lett.* **2004**, *93*, 156801.
[57] H. J. Zhai, J. Li, L. S. Wang, *J. Chem. Phys.* **2004**, *121*, 8369.
[58] J. R. Kitchin, J. K. Nørskov, J. G. Chen, M. A. Barteau, *J. Chem. Phys.* **2004**, *120*, 10240.
[59] W. H. Wang, J. W. Liu, Y. T. Qian, *Chem. Eur. J.* **2005**, *11*, 160.